

Utility of 3D Visualization in Surgical Planning

Khan M. Siddiqui, MD
Chief, Imaging Informatics and Body MR Imaging
VA Maryland Health Care System

10 N. Greene Street, Radiology - 114
Baltimore, MD 21201, USA

Email: ksidd001@umaryland.edu

Case 1: Adult Intussusception

Introduction:

Intussusception is the invagination of one bowel segment (intussusceptum) into an immediately distal bowel segment (intussusciens). It can be classified according to the site of invagination as enteroenteric, colocolic, and enterocolic. By far, the majority of intussusceptions are seen in children under the age of 3 years, in whom it is the second most common abdominal emergency. Intussusception in adults is comparatively rare but often points to significant underlying pathology. An estimated two-thirds of pathologies detected as causes of adult intussusception are benign or malignant neoplasms, and more than half of these neoplasms are malignant⁽¹⁾. As many as 80% of adult patients with intussusceptions are found to have specific causes (lead points), including but not limited to: benign or malignant tumor, lipoma, Meckel's diverticulum, prolapsed gastric mucosa, aberrant pancreas, adhesions, foreign body, feeding tube, chronic ulcer, gastroenterostomy, and trauma. Other causes that may not have an anatomic lead point are celiac disease, scleroderma, Whipple's disease, and anxiety. Untreated intussusception usually progresses to intestinal obstruction, with patients presenting with acute abdominal pain.

In rare cases, the intussusceptum becomes strangulated, necrotic, and gangrenous, leading to peritonitis, sepsis, and death.

The effectiveness of CT in adult intussusception has been recognized for almost a quarter of a century. In the early 1980s, the CT imaging characteristics of intussusception in adult patients were outlined in detail for a range of pathologies^(2,3). Among these characteristics was the marked presence of a "layering" or "stratified" effect, created by areas of high density with curvilinear low-density zones, although this effect could be obscured by edema of the bowel in disease progression^(4,5). During the 1990s, as CT became the imaging modality of choice for the evaluation of patients with abdominal pain, reports of successful early identification and surgical intervention for adult intussusception proliferated⁽⁶⁻⁸⁾. One result was a trend away from attempts to resolve apparent intussusception with non-surgical treatments (e.g., barium enemas) and toward surgical intervention⁽⁹⁾. A recently published multicenter retrospective analysis of 25 years of intussusception cases concluded that surgery is the recommended treatment, with or without a primary reduction of the intussusception⁽¹⁰⁾. However, the same authors reported that despite

improving techniques, abdominal CT identified only 58% of patients found at surgery to have intussusceptions. A smaller study indicated that CT, augmented by abdominal ultrasound, was successful in identifying only 30.7% of such patients before surgery ⁽¹¹⁾.

Despite some suggestions that all adult intussusceptions should be considered surgical emergencies because of the likelihood of significant associated pathologies, the majority of small bowel intussusceptions do not proceed to surgery. Indeed, the association of lead points has been reported to be much lower in small bowel intussusceptions, and several studies have attempted to identify those factors evident on CT that might differentiate cases more or less likely to resolve without surgery ^(12,13). One study reported, for example, that intussusception length was the main factor in CT identification of small-bowel intussusceptions that are self-limiting (<3.5 cm in length) and do not require surgical intervention ⁽¹⁴⁾.

The challenge for the radiologists, then, in using CT for evaluation of adult abdominal pain in the possible presence of intussusception, is three-fold: to identify patients in whom resolution may be achieved through non-surgical procedures, thus avoiding the cost and morbidity associated with surgery; to more accurately identify those patients who have intussusceptions before surgery; and to provide enhanced detail about the intussusception and associated pathologies that may provide valuable information to the surgeon. The classic appearance of intussusception on CT is the target sign or swirling pattern of fat within the two layers of the bowel wall. Although the diagnosis of intussusception may be easy, further characterization of the etiology as well as possible vascular compromise is difficult to assess on axial images. Multi and curved planar reconstruction as well as volume rendered projections provide a better perspective of relationship of various surrounding structures to the loops of bowel involved in the intussusception. 3D visualization also improves the surgeon's understanding of the disease process, enables much better assessment of the vascular supply to the loop of bowel, and helps them to do more effective surgical planning prior to any intervention. ^(15,16)

Case Report:

An 86-year-old woman was referred to our institution for evaluation of acute abdominal pain. CT abdomen and pelvis imaging was performed on a multidetector CT scanner (Somatom 16 scanner; Siemens Medical Solutions, Malvern, PA). After oral administration of 3 × 450 mL of water-soluble oral contrast, CT imaging of the abdomen and pelvis (from the top of the diaphragm to the symphysis pubis) was performed using routine scan parameters (collimation, 0.75 mm; 0.7-mm interval; 120 kVp, 180 mAs; 0.5-sec/rotation). Non-ionic contrast (320 mg/mL iodine for a total of 100 mL at a rate of 4 cc/s) was administered intravenously through a peripheral 16–20-gauge IV cannula. Scan data were then reconstructed at 5-mm thin sections, which were sent to the picture archiving and communications archive (General Electric Medical Systems, Mt. Prospect, IL). The original 0.75-mm thin slices were pushed to the AquariusNET server (TeraRecon, Inc., San Mateo, CA).

Data were then reviewed on the AquariusNET thin-client (TeraRecon, Inc.) in multiplanar (axial, sagittal, and coronal), curved planar, maximum intensity projections, and volume-rendered (VR) formats.

Findings:

Initial reviews without multiplanar reconstructions suggested colonic lymphoma to several imaging specialists (Figure 1). Based on this interpretation, surgical staff recommended endoscopic evaluation of the colon and biopsy for pathologic diagnosis. However,

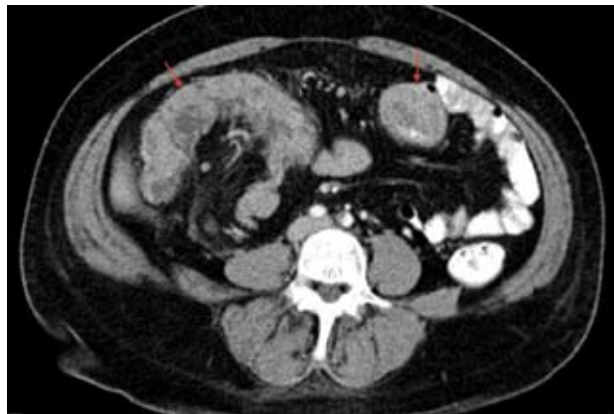


Figure 1 Axial image shows thickened bowel wall (red arrows), but presence of intussusception is difficult to assess.

reviewing images with the AquariusNET thin-client system indicated an ileocolic intussusception extending to the midtransverse colon, marked thickening of the colonic wall, and an enlarged lymph node within the intussuscepted mesentery. No small bowel dilatation was noted, suggesting that small bowel obstruction was not present.

Intraoperative assessment confirmed the CT findings of an ileocolic intussusception. The colon was carpeted with numerous colonic polyps, which in this case constituted the lead point. Several mesenteric nodes were also present. No lead point mass was detected intraoperatively.

Three-dimensional volumetric assessment in this case was crucial in elucidating the relationship between the intussusceptum and the intussusciens. TeraRecon's AquariusNET thin-client allows our physicians to interactively review volumetric data stored on the AquariusNET Server in any viewing format or oblique plane from standard PCs scattered throughout our institution.

Figure 2, for example, shows a curved planar reconstruction through the area of concern, indicating mesenteric fat pushed asymmetrically above the intussusceptum (red arrow). Moreover, this imaging assessment provided significant data on the blood supply and relationship of vessels to the intussusception. Figures 3 and 4 show branches of the superior

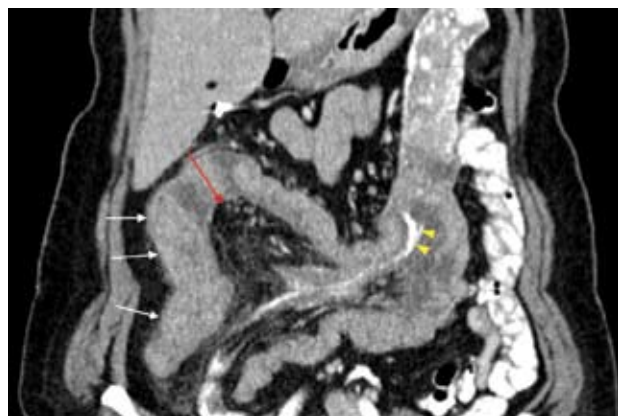


Figure 2: Curved planar reconstruction through the course of the large bowel shows thickened colonic wall (white arrows), mesenteric fat within the intussusception (red arrow) and the ileal intussusceptum (yellow arrowheads).

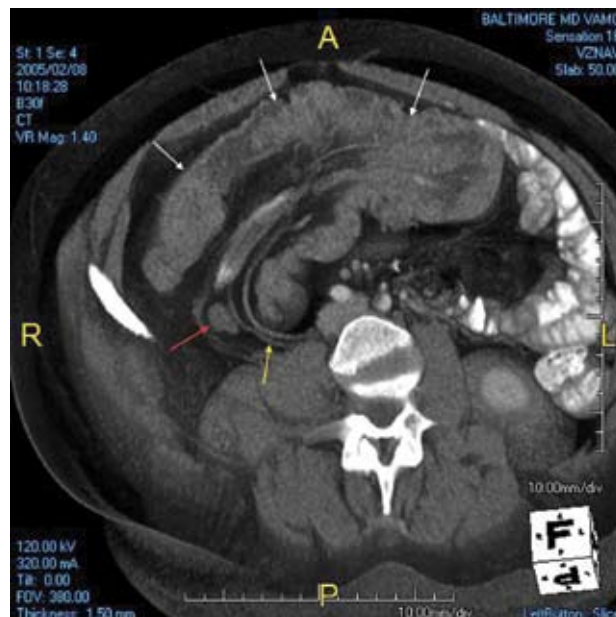


Figure 3: Thick slab volume rendered oblique axial projection shows, thickened colonic wall (white arrows), an enlarged lymph node at the telescoping junction of the intussusception (red arrow) and vascular bundle entering the intussusception (yellow arrow).

mesenteric artery and vein (yellow arrow) entering into the intussusception with the ileal loop (Figure 4, white arrow), along with a lymph node (red arrow)

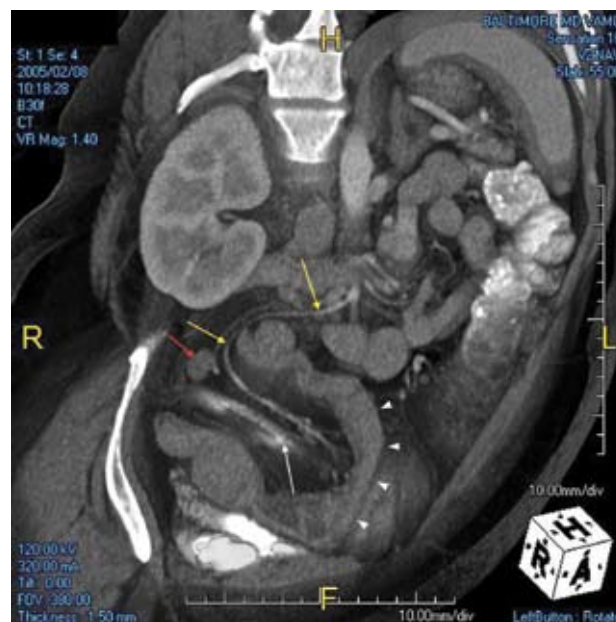


Figure 4: Thick slab volume rendered oblique projection shows, celiac branch of the superior mesenteric artery (yellow arrow) entering with the intussusceptum (white arrow) and an enlarged lymph node (red arrow).

at the telescoping junction of the intussusception. Such preoperative information allows the surgeon to know which vessels are likely to be compromised, to assess the length of the bowel segment that may be ischemic and require resection, and to understand the vascular supply of the affected loops and plan the procedure accordingly.

Conclusion:

In this patient, the addition of 3D volumetric assessment was significant in contributing to a more fully informed progression to surgery. Although much of this imaging information can be visualized on conventional axial images, 3D, VR, multiplanar, and curved planar reconstructions provide quick and clear visualization of the complex relationships of anatomy and pathology, increase our confidence in diagnosis, and contribute to our understanding of the disease process. It is also our experience that these additions to the standard armamentarium of imaging techniques have a strong resonance with both the referring clinician and surgical staff, who find them to be both informative and significant adjuncts in patient management and surgical planning.

References

1. Spalding SC, Evans B. Intussusception. *Emerg Med.* 2004;36:12–19.
2. Parienty RA, Lepreux JF, Gruson B. Sonographic and CT features of ileocolic intussusception. *Am J Roentgenol.* 1981;136:608–610.
3. Styles RA, Larsen CR. CT appearance of adult intussusception. *J Comput Assist Tomogr.* 1983;7:331–333.
4. Iko BO, Teal JS, Siram SM, Chinwuba CE, Roux VJ, Scott VF. Computed tomography of adult colonic intussusception: clinical and experimental studies. *Am J Roentgenol.* 1984;143:769–772.
5. Bar-Ziv J, Soloman A. Computed tomography in adult intussusception. *Gastrointest Radiol.* 1991;16:264–266.
6. Gayer G, Hertz M, Zissin R. CT findings of intussusception in adults. *Semin Ultrasound CT MR.* 2003;24:377–386.
7. Gayer G, Apter S, Hofmann C, et al. Intussusception in adults: CT diagnosis. *Clin Radiol.* 1998;53:53–57.
8. Warshauer DM, Lee JK. Adult intussusception detected at CT or MR imaging: clinical–imaging correlation. *Radiology.* 1999;212:853–860.
9. Sadvovsky R, Marinella MA, Conley CD. Intussusception in an adult. *West J Med.* 1996;165:311–312.
10. Barussaud M, Regenet N, Briennon X, et al. Clinical spectrum and surgical approach of adult intussusceptions: a multicentric study. *Int J Colorectal Dis.* 2005 Jun 11; e-published ahead of print.
11. Erkan N, Hacıyanlı M, Yildirim M, Sayhan H, Vardar E, Polat AF. Intussusception in adults: an unusual and challenging condition for surgeons. *Int J Colorectal Dis.* 2005;20:452–456.
12. Lvoff N, Breiman RS, Coakley FV, Lu Y, Warren RS. Distinguishing features of self-limiting adult small-bowel intussusception identified at CT. *Radiology.* 2004;227:68–72.
13. Sandrasegaran K, Kopecky KK, Rajesh A, Lappas J. Proximal small bowel intussusceptions in adult: CT appearance and clinical significance. *Abdom Imaging.* 2004;29:653–657.
14. Huang BY, Warshauer DM. Adult intussusception: diagnosis and clinical relevance. *Radiol Clin North Am.* 2003;41:1137–1151.
15. Candocia FJ, Goldman I. Three-dimensional computed tomography illustration of small bowel obstruction transition points in patients receiving oral contrast: report of 3 cases. *J Comput Assist Tomogr.* 2005;29(2):202–4.
16. Horton KM, Fishman EK. MDCT of the duodenum: technique and clinical applications. *Crit Rev Comput Tomogr.* 2004;45(5-6):309–34.

CASE 2: Abdominal Aortic Aneurysm

Introduction:

Preoperative imaging has become an important asset in the assessment and treatment of abdominal aortic aneurysm (AAA) (1,2). Although ultrasonography is a cost-effective means of detecting AAA, it does not provide the anatomic delineation necessary for planning aortic repair. Critical information needed for preoperative assessment of AAA includes the relationship of the aneurysm to the renal and supra-renal aortic branches, the degree of iliac arterial involvement with the aneurysm, the presence of other coexisting iliac arterial or aortic aneurysms, the presence of supernumerary or aberrant aortic branches, and the presence of coexistent iliac arterial occlusive disease. In the past, intra-arterial digital subtraction angiography (DSA) was the mainstay of aortic imaging. However, computed tomographic angiography (CTA) has emerged as a minimally invasive alternative to intra-arterial DSA for assessing abdominal, thoracic, and cranial vasculature (3). With the advent

of multidetector CT (MDCT) and robust advanced image visualization tools, CTA has become the gold standard for evaluation of AAA (4-6).

One advantage of CTA is the use of a peripheral intravenous injection of iodinated contrast material compared with the direct arterial injection required in intra-arterial DSA. MDCT enables accurate control of the amount of contrast administered, allowing the imaging specialist to achieve images of superior quality in a fraction of the time and at lower doses of intravenous contrast than previously required (4). The immediately beneficial results are: diminished patient morbidity by eliminating intra-arterial catheterization and substantially reduced times for both the procedure and the requisite post procedural bed rest.

Another important advantage of CTA is that the volumetric data acquired enable the acquisition of views from any angle and perspective, liberating the modal-

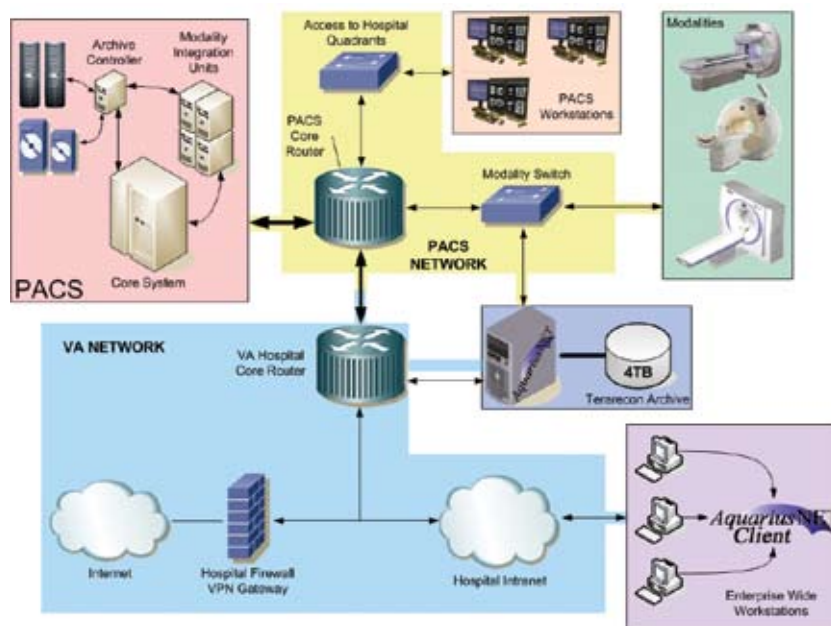


Figure 1 Hospital, PACS, and TeraRecon network layout. Data from modalities is sent to both the PACS and TeraRecon archive. Enterprise wide advanced image visualization is done through AquariusNET Client application installed on all computers on the PACS and hospital networks.

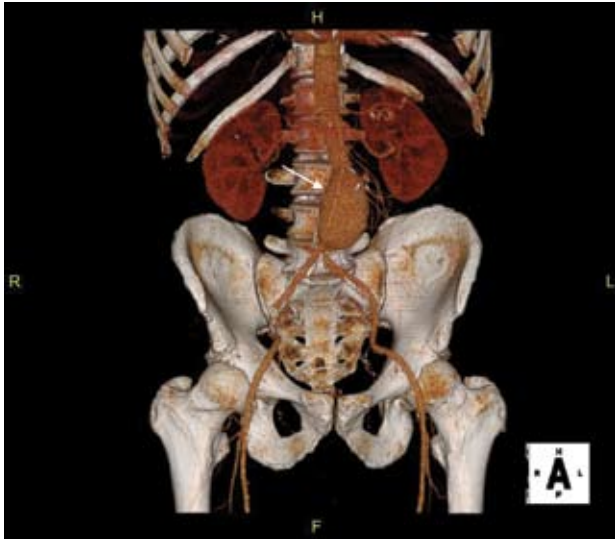


Figure 2 3D volume-rendered image showing the AAA (white arrow).

ity from the limitations of overlap and parallax that plague intra-arterial DSA ⁽⁶⁾. Several reports have indicated the superior diagnostic accuracy of CTA in comparison with intra-arterial DSA in characterizing the neck of the AAA, identifying accessory renal arteries, and characterizing renal arterial stenoses ⁽¹⁰⁻¹²⁾. CTA not only provides information that is equally or more informative than that provided by intra-arterial DSA in some applications but is also less costly ⁽²⁾.



Figure 3: Slab volume-rendered image showing the relationship of aneurysmal sac (white arrow) with the origins of the renal arteries (yellow arrows) and the intramural thrombus (red arrows).

This case study details the example of a 51-year-old man who was referred for imaging evaluation of a pulsatile abdominal mass incidentally palpated by the primary care physician during a routine annual physical examination.

Case Report:

The 51-year-old patient was scheduled to undergo CTA. At our institution, CTA for evaluation of AAA was performed on an MDCT scanner (Somatom 16 scanner; Siemens Medical Systems, Malvern, PA). The protocol for presurgical planning included an initial noncontrast CT of the abdomen and pelvis (from the top of the diaphragm to the symphysis pubis; collimation of 0.75 mm; 0.7-mm interval; 120 kVp, 180 mAs; 0.5-s/rotation). This was followed by contrast-enhanced CT of the abdomen with the following scan parameters: collimation of 0.75 mm; 0.7-mm interval; 120 kVp, 180 mAs; 0.5-s/rotation. Non-ionic contrast (320 mg/mL iodine for a total of 100 mL at a rate of 4 cc/s) was administered intravenously through a peripheral 16–20 gauge IV cannula. Automated bolus tracking was used to optimize contrast density in the aorta with the region of interest in the descending thoracic aorta. Data for both acquisitions was then reconstructed at 5-mm thin sections, which were sent to the picture archiving and communications system archive (General Electric Medical Systems; Mt. Prospect, IL). The original 0.75-mm thin slices were pushed to the AquariusNET server (TeraRecon Inc.; San Mateo, CA). Network layout and data transmission route are shown in Figure 1.

Data were then reviewed on the AquariusNET Client (TeraRecon, Inc.) in multiplanar (axial, sagittal, and coronal), curved planar, maximum intensity projections, and volume-rendered (VR) formats. Automated vessel analysis tools were used to assess the dimensions of the AAA.

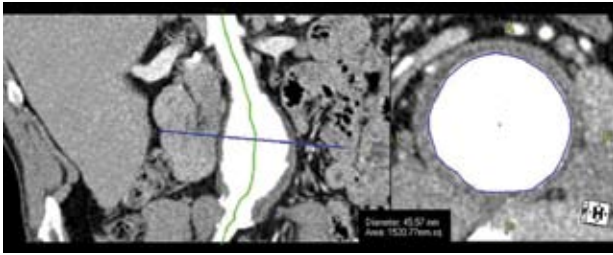


Figure 4: Vessel review layout during automated vessel analysis shows maximum aortic diameter of 45.57mm (area = 1520.77mm²).

Findings:

The initial color VR image (Fig. 2) shows atherosclerotic calcifications of the right external iliac artery as well as the relationship of the aneurysm with the aortic bifurcation. Based on these findings, the right femoral approach would not be ideal for initial canalization of the right external iliac artery. The renal arteries are seen to originate from the normal portion of the abdominal aorta, which is much higher than the proximal part of the aneurysm as seen on the grayscale VR image (Fig. 3). Figure 3 also shows the relationship of the mural thrombus to the aneurysm wall.



Figure 6 Postoperative slab volume-rendered image shows successful deployment of the endovascular graft (red arrows).

Curved planar reconstruction was performed to assess the true cross-sectional diameter of the aneurysm (Fig. 4). Two points initially were selected proximal and distal to the aneurysm, following the automated vessel centerline extraction. The vessel view layout shows a maximum cross-section diameter of 45.57 mm perpendicular to the vessel centerline.

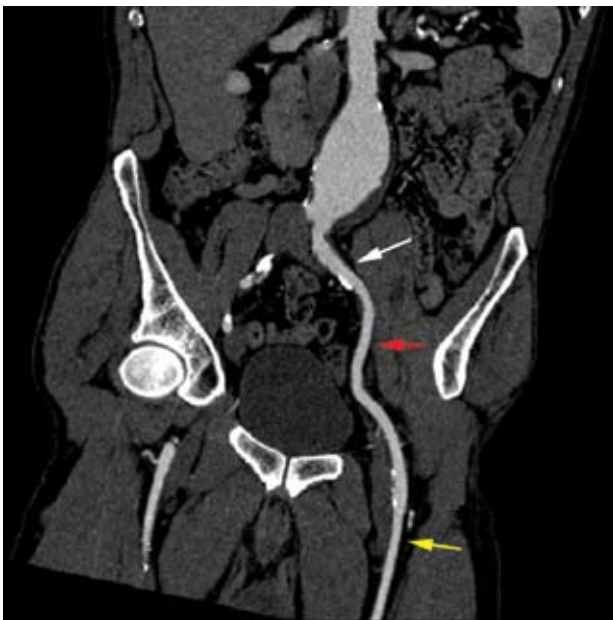


Figure 5 Curved planar reconstruction through the left common iliac (white arrow), external iliac (red arrow) and superficial femoral arteries (yellow arrow).



Figure 7 3D volume-rendered image shows the endovascular graft (red arrows).

Curved planar reconstruction also was performed to assess the patency of the left common iliac, left external iliac, and left superficial femoral arteries (Fig. 5), which show no significant disease. Therefore, the left femoral approach was used for the deployment of the endovascular graft. Postoperative noncontrast CT examination (Figs. 6 and 7) demonstrate successful deployment of the endoluminal vascular graft.

Conclusion

The latest advances in MDCT and 3D VR have much to offer in the evaluation of AAA. VR is suitable for augmenting the already clear advantages of high-quality MDCT data and, because of the increasing size of the datasets involved, can be considered a necessity. Not only does this technique expand the established conventional roles of vascular CT, but it shows great potential in a host of other novel applications ⁽⁶⁾.

References

1. Verbin C, Scoccianti M, Kopchok G, Donayre C, White RA. Comparison of the utility of CT scans and intravascular ultrasound in endovascular aortic grafting. *Ann Vasc Surg.* 1995;9:434–440.
2. Rubin GD, Armerding MD, Dake MD, Napel S. Cost identification of abdominal aortic aneurysm imaging by using time and motion analyses. *Radiology.* 2000;215:63–70.
3. Rubin GD, Dake MD, Napel S, Jeffrey RBJ. Three-dimensional CT angiography as an alternative to conventional arteriography in planning and in vivo evaluation of aortic stent grafts [abstract]. *Radiology.* 1993;189(P):112.
4. Ho LM, Nelson RC, Thomas J, Gimenez EI, DeLong DM. Abdominal aortic aneurysms at multi-detector row helical CT: optimization with interactive determination of scanning delay and contrast medium dose. *Radiology.* 2004;232:854–859.
5. Rubin GD, Shiao MC, Leung AN, Kee ST, Logan LJ, Sofilos MC. Aorta and iliac arteries: single versus multiple detector-row helical CT angiography. *Radiology.* 2000;215:670–676.
6. Lawler LP, Fishman EK. Multi-detector row CT of thoracic disease with emphasis on 3D volume rendering and CT angiography. *RadioGraphics.* 2001;21:1257–1273.